Tuning the properties of complex transparent conducting oxides: Role of crystal symmetry, chemical composition, and carrier generation

Julia E. Medvedeva[*] and Chaminda L. Hettiarachchi

Department of Physics, Missouri University of Science and Technology, Rolla, Missouri 65409, USA
(Received 18 December 2009; revised manuscript received 24 February 2010; published 17 March 2010)

The electronic properties of single- and multication transparent conducting oxides (TCOs) are investigated using first-principles density-functional approach. A detailed comparison of the electronic band structure of stoichiometric and oxygen deficient In_2O_3, α, and β-Ga_2O_3, rock salt and wurtzite ZnO, and layered $InGaZnO_4$ reveals the role of the following factors which govern the transport and optical properties of these TCO materials: (i) the crystal symmetry of the oxides, including both the oxygen coordination and the long-range structural anisotropy; (ii) the electronic configuration of the cation(s), specifically, the type of orbital(s)—s, p, or d—which form the conduction band; and (iii) the strength of the hybridization between the cation's states and the p states of the neighboring oxygen atoms. The results not only explain the experimentally observed trends in the electrical conductivity in the single-cation TCO, but also demonstrate that multicomponent oxides may offer a way to overcome the electron localization bottleneck which limits the charge transport in wide band-gap main-group metal oxides. Further, the advantages of aliovalent substitutional doping—an alternative route to generate carriers in a TCO host—are outlined based on the electronic band structure calculations of Sn, Ga, Ti, and Zr-doped $InGaZnO_4$. We show that the transition metal dopants offer a possibility to improve conductivity without compromising the optical transmittance.

I. INTRODUCTION

Multicomponent transparent conducting oxides (TCOs)—complex oxides which contain several types of main group metal ions—have been developed[1–6] to broaden the range of transparent conducting and semiconducting materials required for a variety of applications, including photovoltaic cells, flat panel displays, and flexible and invisible electronics. Binary and ternary compounds and solid solutions with electrical, optical and mechanical properties controlled via chemical composition, have been a subject of numerous investigations, e.g., see Refs. [2–6] for reviews. Since the 1990s, the multication TCOs which include metal ions beyond the traditionally employed Sn, Cd, In and Zn have emerged, for example, $MgIn_2O_4$,[7] $GaInO_3$,[8] and the so-called 2-3-3 or 3-3-4 systems where the numbers correspond to divalent, trivalent and tetravalent cations.[9] Among them, layered compounds of the homologous series $(In,Ga)_2O_3(ZnO)_n$, where n=integer, attract an increasing attention,[10–22] originally, due to a possibility to enhance conductivity via spatial separation of the carrier donors (dopants) located in insulating layers and the conducting layers which transfer the carriers effectively, i.e., without charge scattering. However, the electrical conductivity and carrier mobility observed to date in these complex materials, σ=100–400 S/cm and μ=10–20 cm^2/V·s, respectively,[10,12,15,23–25] are considerably lower than those achieved in the single-cation TCOs such as In_2O_3, SnO_2, or ZnO, with σ=10^3–10^4 S/cm and μ=50–100 cm^2/V·s.

The low conductivity in $(In,Ga)_2O_3(ZnO)_n$ which decreases continuously as the number of ZnO layers, n, increases, along with the observed strong anisotropy of the transport properties in these complex oxides[13,15] was assumed to correlate with the density of the octahedrally coordinated In atoms that changes with n. Since late 1970s, the octahedral oxygen coordination of cations was believed to be essential for a good transparent conductor.[1,6,9,26,27] Accordingly, it has been suggested that in $(In,Ga)_2O_3(ZnO)_n$ the charge is transferred only within the octahedrally coordinated In layers while the Ga-Zn layers where both cations have tetrahedral oxygen coordination, were believed to be nonconducting.[10,28] However, the above assumption appears to be in conflict with:

(i) experimental observations that the mobility and conductivity are independent of the compositional variations in the *amorphous* $InGaO_3(ZnO)_n$ and the conclusion that this material is a Zn 4s conductor,[25]

(ii) electronic band-structure investigations which showed that all chemically and structurally distinct layers in $InGaZnO_4(n$=1) and in similar compounds are expected to participate in the charge transport owing to the hybrid nature of the bottom of the conduction band formed from the s states of *all* cations in the cell and the p states of their oxygen neighbors.[29]

The above discrepancy calls for further microscopic analysis of the layered oxides. In particular, the underlying mechanisms associated with carrier generation in the complex TCO materials should be addressed. The purpose of this work is not only to determine the properties of oxygen deficient or substitutionally doped $InGaZnO_4$ but also to understand how the presence of several cations of different valence, ionic size, electronic configuration, and oxygen coordination affects the carrier generation and the overall electronic and optical properties of complex TCOs.

For the materials of the $(In,Ga)_2O_3(ZnO)_n$ family, it has been accepted that free carriers appear due to the formation of oxygen vacancies. Also, it was assumed that each vacancy donates two extra electrons, i.e., there is no charge compensation via natural defects or defect complexes. However, it was shown theoretically[30] that uncompensated oxygen va-

cancy in $InGaZnO_4$ results in a deep level within the band gap and, thus, free carriers cannot be efficiently generated. Therefore, oxygen vacancy cannot explain the observed conducting behavior in this material.

Substitutional doping, an alternative route to generate carriers, remains unexplored in $InGaZnO_4$ and the compounds of the homologous series. One of the main reasons for this is the structural and compositional complexity of multicomponent oxides. Indeed, the presence of several cations with different valence (e.g., In^{3+} and Ga^{3+} vs Zn^{2+}) and oxygen coordination (octahedral for In vs tetrahedral for Ga and Zn) may facilitate a nonuniform distribution of impurities including their clustering or secondary phase formation. Furthermore, targeted doping required for extra carrier generation via aliovalent substitution, becomes difficult as the number of the structurally and/or chemically distinct cations in the complex material increases. The aliovalent substitutional dopants known to be efficient carrier donors in the constituent single-cation TCO, e.g., Al^{3+} in ZnO, may not be suitable for the complex oxides since they may prefer to substitute the cations of the same valence (In^{3+} or Ga^{3+}). In this case, extra carriers are not generated. Formation of charge compensating defects and defect complexes is also more likely in complex oxides. Thus, the range of dopants which are efficient for a given multicomponent material may be quite narrow.

In this work, first-principles density-functional approach is employed to investigate possible carrier generation mechanisms in the layered $InGaZnO_4 (n=1)$ and its constituent single-cation oxides, In_2O_3, Ga_2O_3, and ZnO, and to understand how each of the mechanisms affects the resulting electronic and optical properties. First, we perform electronic band-structure calculations of oxygen deficient materials to understand the origin of the observed anisotropic transport properties in the layered multicomponent oxide. For this, we analyze the role of crystal symmetry and metal-oxygen hybridization by comparing the properties of high- and low-symmetry oxide phases. In addition, our comparative studies of several oxides allow us to understand how chemical composition (In vs Zn vs Ga oxides) affects the resulting optical and electronic properties.

Next, in search of efficient substitutional dopants, we study the structural and electronic properties of $InGaZnO_4$ doped with either conventional dopants such as the post-transition metal ions (Sn, Ga) or with the transition metals (Ti, Zr). We find that the optical and transport properties are both sensitive to the ionic radius of the dopant and its electronic configuration. In particular, we show that the presence of the localized d states is beneficial for balancing good conductivity with low optical absorption. Based on the results obtained, the (dis)advantages of both carrier generation mechanisms—oxygen reduction and aliovalent substitutional doping—are discussed. We conclude that the conductivity currently achieved in the oxygen deficient $(In,Ga)_2O_3(ZnO)_n$ can be significantly improved with proper doping of the host material.

The paper is organized as follows. First, theoretical approaches and structural peculiarities of the compounds under investigation are outlined in Sec. II. Studies of oxygen deficient In_2O_3, α, and β-Ga_2O_3, rocksalt and wurtzite ZnO are

presented in Sec. III. Here we discuss the formation energies of the oxygen vacancy in various charge states and the changes in the host electronic band structure caused by the presence of the oxygen defect. Significantly, the range of materials investigated allows us to address the long-standing question about the role of the crystal symmetry, both local (oxygen coordination) and long-range (structural anisotropy), in the charge transport. In addition, we compare the electronic band structure features of the three oxides and draw general conclusions about the role of the cation-anion orbital hybridization in the resulting transport properties. In Sec. IV, we perform similar investigations for the layered undoped stoichiometric and oxygen deficient $InGaZnO_4$.

In Sec. V, aliovalent substitutional doping is considered. For each of the dopants studied, i.e., Sn, Ga, Ti, or Zr, several distinct site locations in the layered $InGaZnO_4$ are compared based on the total energy calculations. The results, along with the considerations of the dopant and the substituted cation valences, allow us to judge the efficiency of each dopant, i.e., its capability to donate extra electrons. Further in this section, the role of the dopant electronic configuration in both the transport and optical properties is discussed and practical ways to optimize the former without compromising the latter are outlined. Finally, calculations for $InGaZnO_4$ with interstitial oxygen atoms located within either the In-O or Ga-Zn-O layers are performed to investigate a possibility of charge compensation in substitutionally doped materials.

We discuss the implications of the obtained results in Sec. VI.

II. APPROACH

First-principles full-potential linearized augmented plane wave method[31,32] with the local density approximation (LDA) is employed for the electronic band structure investigations. Cutoffs for the basis functions, 16.0 Ry, and potential representation, 81.0 Ry, and expansion in terms of spherical harmonics with $\ell \leq 8$ inside the muffin-tin spheres were used. The muffin-tin radii are 2.3 for In; 1.85 a.u. for Ga; 1.9 for Zn; and 1.6 a.u. for O atoms. Summations over the Brillouin zone were carried out using at least 23 special **k** points in the irreducible wedge. For every structure investigated, the internal positions of atoms were optimized via the total energy and atomic forces minimization.

To study the electronic properties of undoped stoichiometric oxides, we also employed the self-consistent screened-exchange LDA (sX-LDA) method[33–37] for more accurate description of the band gap values and the valence/conduction band edges. The sX-LDA is known to provide a better energy functional beyond LDA or generalized gradient approximation by modeling the exchange-correlation hole within the *nonlocal* density scheme.

$InGaZnO_4$ has rhombohedral $R\bar{3}m$ crystal structure of $YbFe_2O_4$ type.[38,39] Indium atoms reside in the 3(a) positions (Yb), while both Ga^{3+} and Zn^{2+} atoms are in the 6(c) positions (Fe) and are distributed randomly[40]—as confirmed by our total energy calculations.[29] Because of the different ionic radii, the Ga and Zn atoms have different z component of the internal site position $(0,0,z)$: we find $z=0.214$ for Ga and

TABLE I. Structural and electronic properties of TCO hosts—the undoped stoichiometric oxides. The values are determined within the self-consistent screened-exchange local-density approximation and within LDA (given in parentheses). Anisotropy of the electron effective mass is defined as $\delta = (m^{[100]} + m^{[010]})/2m^{[001]}$.

| Lattice | In$_2$O$_3$ | ZnO | | Ga$_2$O$_3$ | | InGaZnO$_4$ |
	Bixbyite	Wurtzite	Rocksalt	Monoclinic	Corundum	Rhombohedral
Coordination of cation	6	4	6	6,4	6	6(In),4(Zn,Ga)
Coordination of anion	4	4	6	4,3	4	4
Fundamental gap, eV	2.88 (1.16)	3.41 (0.81)	2.49 (1.03)	4.86 (2.32)	5.16 (2.81)	3.29 (1.19)
Optical (direct) band gap, eV	3.38 (1.52)	3.41 (0.81)	3.86 (2.28)	4.91 (2.32)	5.40 (3.06)	3.40 (1.28)
Electron effective mass, in m$_e$	0.28 (0.18)	0.35 (0.19)	0.28 (0.22)	0.34 (0.24)	0.32 (0.23)	0.34 (0.21)
Effective mass anisotropy, δ	1.00 (1.00)	1.01 (1.25)	1.00 (1.00)	1.10 (1.23)	1.00 (1.00)	1.00 (0.97)

$z = 0.218$ for Zn. The optimized cation-anion distances are 2.16–2.22 Å for In-O; 1.88 Å and 1.96–2.16 Å for the Ga-O in the *ab* plane and along the [0001] direction, respectively; and 1.97 and 1.99–2.36 Å for the planar and apical Zn-O distances, respectively. These values correlate with the ionic radii of the cations (0.94 Å for six-coordinated In, 0.61 Å for four-coordinated Ga and 0.74 Å for four-coordinated Zn) and correspond to the cation-anion distances in the single-cation oxides, i.e., In$_2$O$_3$(2.13–2.25 Å), Ga$_2$O$_3$ (1.83–2.07 Å), and ZnO (1.97–2.14 Å).

To model isolated point defects, the following supercells were constructed: a 49-atom supercell with the lattice vectors $(30\bar{2})$, $(\bar{1}12)$, and $(02\bar{1})$, given in the units of the rhombohedral primitive cell vectors and a 77-atom supercell with the lattice vectors $(30\bar{2})$, $(\bar{1}3\bar{1})$, and $(\bar{2}12)$ for InGaZnO$_4$; a 40-atom and 80-atom supercells for bixbyite In$_2$O$_3$; a 120-atom supercell for monoclinic β-Ga$_2$O$_3$; a 80-atom supercell for rhombohedral (corundum) α-Ga$_2$O$_3$; a 84-atom supercell with the lattice vectors $(\bar{2}\bar{2}1)$, $(\bar{1}31)$, and $(2\bar{3}1)$, given in the units of the hexagonal primitive cell vectors for wurtzite ZnO; and 64 and 128-atom supercells for cubic ZnO.

To compare the properties of oxides, we choose the supercells which result in a similar defect concentration, namely, 0.8–1.0×10^{21} cm^{-3}. This corresponds to the distance between the oxygen defects of 8–10 Å. We stress that such high concentrations may not be experimentally feasible in all materials under consideration. However, our goal is (i) to compare the properties in oxides under the same (perhaps, hypothetical) conditions and (ii) to demonstrate that even when the defects are relatively close to each other in our model and so their wave functions are expected to overlap significantly and, hence, form a broad band, we obtain a localized state (as, for example, in β-Ga$_2$O$_3$, see below).

The oxygen vacancy with three charge states, i.e., neutral V$_O^0$ and ionized V$_O^+$ or V$_O^{2+}$, was modeled using a corresponding background charge. The defect formation energy is calculated as

$$\Delta H(E_F, \mu) = E_{defect} - E_{host} + \sum \pm (\mu^0 + \Delta\mu) + qE_F, \quad (1)$$

where E_{defect} and E_{host} are the total energies for the oxygen deficient oxide and the stoichiometric oxide in the same-size supercell, respectively; $\Delta\mu$ is the chemical potential for atom added to (−) or removed from (+) the lattice; q is the defect charge state and E_F is the Fermi energy. The chemical potentials $\Delta\mu$ are taken with respect to the LDA energy μ^0 of the elementary metals or the O$_2$ molecule. We apply the thermodynamic stability condition for the oxides. Our calculated formation enthalpies, ΔH_f, are in a good agreement with the experimental values given in parenthesis: $\Delta H_f(\text{In}_2\text{O}_3) = -8.2$ eV(−9.6 eV); $\Delta H_f(\text{ZnO}) = -3.4$ eV(−3.6 eV); $\Delta H_f(\text{Ga}_2\text{O}_3) = -9.7$ eV(−11.2 eV); and $\Delta H_f(\text{InGaZnO}_4) = -11.97$ eV (experimental data not available). The formation energies of substitutionally doped In$_2$O$_3$ and InGaZnO$_4$ were calculated with respect to the bulk orthorhombic Ga, tetragonal In and Sn, and hexagonal Ti, Zr, and Zn metals.

III. ELECTRONIC PROPERTIES OF In$_2$O$_3$, Ga$_2$O$_3$, AND ZnO

A. Undoped stoichiometric TCO hosts

Oxides of post-transition metals with $(n-1)d^{10}ns^2$ electronic configuration, such as In$_2$O$_3$, Ga$_2$O$_3$, ZnO, and CdO share similar chemical, structural, and electronic properties. They have densely packed structures with four- or six-coordinate metal ions, Table I. Strong interactions between the oxygen 2p and metal ns orbitals give rise to electronic band structures which are qualitatively similar among all of these oxides, Fig. 1, the bonding and nonbonding O 2p states form the valence band while the conduction band arises from the antibonding Ms-Op interactions where M stands for metal ion. The empty p states of the cation (dashed line) form the following band at a higher energy. The partial density of states plots, Fig. 1, reveal that the oxygen 2p (thin line) and metal ns (thick line 3) states make similar contributions to the conduction band. This provides a three-dimensional Ms-Op network for charge transport once extra carriers fill the band.[41]

Ms-Op interactions result in a gap between the valence and the conduction bands. In ZnO, the gap is direct whereas in In$_2$O$_3$ and Ga$_2$O$_3$ the valence-band maximum is at the H point ([$1\bar{1}1$]) and M point ([$\bar{1}11$]), respectively, giving rise to indirect band gap of 2.88 and 4.86 eV, respectively. (For results on CdO, see Refs. 42–45.) For TCO applications, direct optical band gaps are of primary importance. The calculated values are given in Table I. As one can see, our
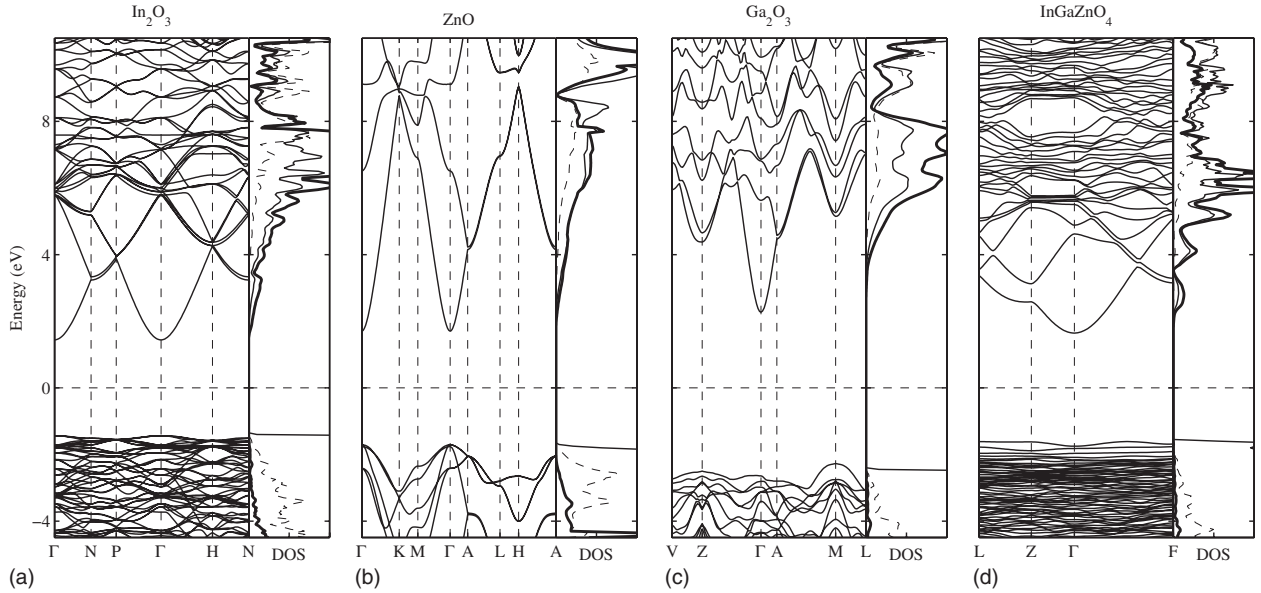
FIG. 1. Electronic band structure and DOS of undoped stoichiometric (a) bixbyite In_2O_3, (b) wurtzite ZnO, (c) monoclinic Ga_2O_3, and (d) layered $InGaZnO_4$ as calculated within the self-consistent sX-LDA. The thick, dashed, and thin lines in the DOS plots represent the metal s, metal p, and oxygen p states, respectively.

sX-LDA results are in excellent agreement with the reported experimental and theoretical values, namely, 2.9 eV for the fundamental band gap and 3.5–3.7 eV for the optical band gap for In_2O_3,[46–49] 3.1–3.6 eV for ZnO[50] and 4.5–4.9 eV for Ga_2O_3,[51,52] while LDA significantly underestimates the band gap values, as expected.

The Ms-Op overlap also determines the energy dispersion of the conduction band in these materials. Within the framework of $\mathbf{k} \cdot \mathbf{p}$ theory,[53] the electron effective mass can be found within the second-order perturbation

$$\frac{m_e}{m_{ii}^{(c)}} = 1 + \frac{2}{m_e} \sum_{l \neq c} \frac{|\langle u^{(c)} | \hat{p}_i | u^{(l)} \rangle|^2}{E^{(c)} - E^{(l)}}, \qquad (2)$$

where $\hat{\mathbf{p}}$ is the momentum operator, $|u^{(l)}\rangle$ is the Bloch wave function of the l's band at the Γ point (wave vector $\mathbf{k}=0$), and $E^{(l)}$ is its energy. Band label c represents the conduction band, while the sum runs over all other bands. In the oxides under consideration here, the electron effective mass is less than the mass of the electron, m_e. As it follows from Eq. (2), it is determined primarily by the valence-band contributions ($E^{(l)} < E^{(c)}$), i.e., by the oxygen $2p$ states. Thus, the network of alternating metal and oxygen atoms ensures the small electron effective mass in the TCO hosts.[41]

Moreover, the electron effective mass varies insignificantly with oxygen coordination which may be different for different phases of the same-cation oxide.[29] For example, for ZnO in rock salt (octahedral coordination) or wurtzite (tetrahedral coordination) structures, and for In_2O_3 in $Ia\bar{3}$ (bixbyite), $R\bar{3}c$ (corundum) or $I2_13$ structures, the effective masses vary by less than or about 15% (see also Ref. 49). In addition, the effective mass remains nearly isotropic in all oxide phases considered including those with well-defined long-range structural anisotropy. This is in accord with the investigations of complex oxides of main group metals[29,54] where

isotropic electron effective mass is found for oxides with irregular atomic arrangements or large structural voids. These observations explain the success of (i) amorphous TCOs whose electrical properties remain similar to those in the crystalline state and (ii) TCO-based flexible transparent conducting coatings.

As shown in the next section where we consider the conversion of the undoped stoichiometric TCO hosts from insulators into conductors, the Ms-Op origin of the conduction band plays critical role in determining the resulting transport properties.

B. Oxygen deficient In_2O_3, ZnO, and Ga_2O_3

Oxides of post-transition metals exhibit a relatively low free energy of formation[55] which favors large oxygen deficiencies even under equilibrium growth conditions. This gives rise to the free-carrier densities as large as 10^{17}–10^{19} cm^{-3} in In_2O_3, and ZnO.[56–58]

Removal of an oxygen atom from the metal oxide leaves two extra electrons in the crystal. Whether one or both of these electrons become mobile (free) carriers or remain localized at the vacancy site is determined by the formation energy of the oxygen defect which can have various charge states (i.e., V_O^0, V_O^+, or V_O^{2+}). We find that in all oxides investigated in this work, the neutral oxygen defect V_O^0 corresponds to the ground state of the oxygen vacancy, Fig. 2. This is in accord with the results for In_2O_3 and ZnO by Lany and Zunger.[58] From the electronic band-structure calculations for oxygen deficient In_2O_3, Ga_2O_3, and ZnO, we find that the uncompensated oxygen vacancy, V_O^0, gives rise to a fully occupied (by the two vacancy-induced electrons), thus, nonconductive state, as the Fermi level falls into a gap between the defect state and the rest of the conduction band.

The observed conductivity in In_2O_3 and ZnO was attributed to the photoexcited oxygen vacancy, i.e., V_O^{1+}, which
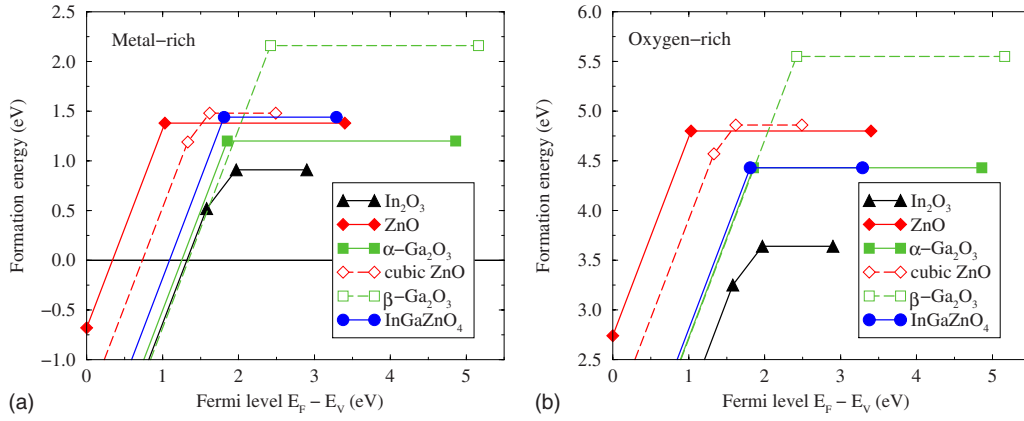
FIG. 2. (Color online) Calculated formation energies of the oxygen vacancy as a function of the Fermi level. The symbols indicate the transition energies between different charge states of the oxygen defect. Solid lines stand for In_2O_3 (triangles), wurtzite ZnO (diamonds), monoclinic β-Ga_2O_3 (squares), and $InGaZnO_4$ (circles). Dashed lines are for rocksalt ZnO (open diamonds) and rhombohedral α-Ga_2O_3 (open squares). The oxygen defect concentration in all systems is $0.8-1.1\times10^{21}$ cm^{-3}. The results are obtained within LDA.

provides a metastable conductive state.[58] Indeed, when the oxygen vacancy is singly ionized (V_O^+), the lowest *single* conduction band associated with the presence of the oxygen defect becomes half occupied, leading to a conducting behavior.[59] Within the LDA, we estimate the optical excitation $V_O^0 \rightarrow V_O^+ + e^-$ to be 1.64, 1.48, and 2.02 eV for In_2O_3, ZnO, and Ga_2O_3, respectively. These values are underestimated because LDA underestimates the band gap by 2–3 eV, cf. Table I.

Thus, only if the oxygen vacancy is excited to V_O^+, a conducting behavior may occur. The conductive state associated with V_O^+ is found to be located closer to the conduction-band minimum (CBM) as compared to V_O^0, Table II. Again, the values in Table II for the location of the defect states with respect to band edges may be underestimated, however, we expect that LDA captures the trend among the oxides[60] and below we use the LDA results to compare with those obtained for oxygen deficient α-Ga_2O_3, rock salt ZnO, and $InGaZnO_4$.

Despite similar defect concentration and, hence, similar distance between the oxygen defects (8–10 Å) in In_2O_3, ZnO, and β-Ga_2O_3, the obtained widths of the lowest conduction band in the conductive oxides (i.e., those with V_O^+ defect) differ significantly, Table II. The lower-energy dispersion of the conduction band in β-Ga_2O_3 suggests that the extra electrons tend to localize—in marked contrast to the extended state in In_2O_3. Accordingly, the calculated Fermi electron group velocities in the conductive oxides differ by almost an order of magnitude, Table II. We stress that these differences cannot be accounted by the variation in the electron effective masses of stoichiometric materials (cf. Table I). The obtained trend in the electron group velocities is in accord with experimental results: indium oxide is known to be the best TCO in terms of the minimum resistivity achieved, whereas β-Ga_2O_3 has not been considered as a viable TCO and, moreover, is believed to be the constituent detrimental for the charge transport of a multicomponent oxide. To understand the microscopic origin of the different

TABLE II. Electronic properties of oxygen deficient In_2O_3, wurtzite and rock-salt ZnO, α-Ga_2O_3 and β-Ga_2O_3, and $InGaZnO_4$ as calculated within LDA. The conduction-band width reflects the degree of electron localization. The smaller the s-orbital contribution on the cations nearest to the oxygen vacancy, the more charge stays trapped near the defect.

|	In_2O_3	h-ZnO	β-Ga_2O_3	c-ZnO	α-Ga_2O_3	$InGaZnO_4$
Oxygen defect concentration, $\times10^{21}$ cm^{-3}	0.97	1.00	0.80	0.80	1.30	1.11
Distance between the defects, Å	10	8	9	12	11	11
Location of nonconducting V_O^0 state below CBM, eV	0.57	0.82	1.81	0.47	1.82	0.47
Optical exitation $V_O^0 \rightarrow V_O^+ + e^-$, eV	1.64	1.48	2.01	1.68	2.19	1.64
Location of metastable conducting V_O^+ state below CBM, eV	0.38	0.35	1.39	0.49	0.88	0.31
For conducting oxides, i.e., those with V_O^+ defect Conduction band width, eV	1.56	0.96	0.45	1.16	0.65	1.14
Electron velocity at Fermi level, $v_{BZ}\times10^5$ m/s	6.67	3.91	0.96	6.47	2.35	4.76
Direction of v_{BZ} in standard Brillouin zone	$[1\bar{1}1]$	$[100]$	$[\bar{1}10]$	$[110]$	$[110]$	$[110]$
Charge build-up at defect neighbors, %	31	39	61	27	53	37
Nearest cations s-orbital contribution, %	81	71	56	82	66	82(In), 74(Zn)
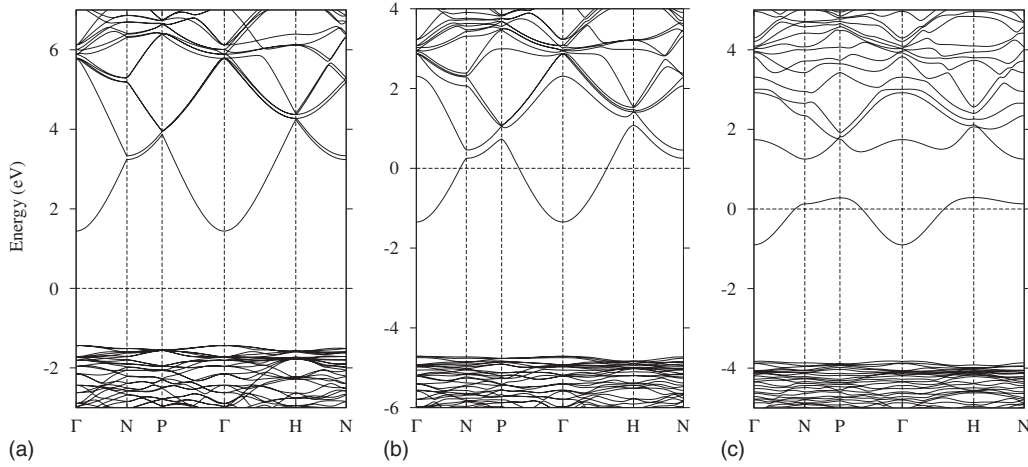
FIG. 3. Electronic band structure of (a) undoped stoichiometric In_2O_3, (b) 6.25 at.% Sn-doped In_2O_3 which corresponds to Sn concentration of 1.93×10^{21} cm^{-3}, and (c) oxygen deficient In_2O_3 with the oxygen vacancy V_O^+ concentration of 1.96×10^{21} cm^{-3} as obtained within self-consistent sX-LDA.

electronic properties of the oxygen deficient oxides, further comparative analysis will follow (see Secs. III C–III E).

At the end of this section, we would like to point out the differences in the electronic band structures of oxygen deficient and substitutionally doped oxides. Figure 3 illustrates how the electronic band structure of the In_2O_3 host is affected by the presence of oxygen vacancy (V_O^+) or substitutional Sn atom (Sn_{In}). For the same concentration and the same charge state of the two defects, we find that oxygen vacancy leads to a nonrigid-band shift of the Fermi level, and a large second gap appears due to the splitting of the lowest single conduction band from the rest of the conduction band, Fig. 2. Conversely, there is no second gap in the case of Sn substitution. We have found earlier[61] that the second gap previously reported (Ref. 62) for Sn-doped In_2O_3 vanishes upon structural relaxation around Sn ions. In marked contrast to the substitutional doping, the second gap *increases* by about 23% when the structure of the oxygen deficient In_2O_3 is allowed to fully relax. Indeed, the absence of a second gap in case of the substitutional doping indicates a good hybridization of the dopant states (Sn s states) with the states of the neighboring atoms (O p states), while an oxygen vacancy implies a substantial redistribution of the electron density to accommodate the defect and to minimize its impact. The obtained differences in the structure of the conduction band bottom of the doped and oxygen deficient oxide will, clearly, give rise to different transport and optical properties.

C. Electron localization in oxygen deficient TCO

Our goal is to understand the microscopic origin of the different electronic properties (cf. Table II) of the three oxides in which the cations have the same electronic configuration, i.e., s^0p^0. In particular, we would like to understand the origin of the strong electron localization that manifests itself in the narrow conduction band in oxygen deficient β-Ga_2O_3. For this, we analyze the charge density distribution within the lowest conduction band and also compare the contributions to the conduction band from the cations and anions

located at different distances from the oxygen defect.

For In_2O_3 we find that the In atoms nearest to the vacancy site give 2–3 times larger contributions than the rest of the In atoms in the cell. As a result, there is a notable build-up of the charge density near the vacancy, namely, 31% of the total charge at the bottom of the conduction band reside on the nearest-neighbor In and the next-nearest-neighbor O atoms.

In oxygen deficient ZnO, there is an order of magnitude difference between the contributions from the specific atoms (either cations or anions) and 39% of the total charge density belong to the nearest Zn and next nearest O neighbors of the oxygen vacancy.

In Ga_2O_3 we find that 61% of the total charge is at the defect's nearest-neighbor cations and the next-nearest-neighbor oxygen atoms, with the rest of the cations or anions giving up to two orders of magnitude smaller contributions.

Thus, the electron density distribution is more uniform within the cell in indium and zinc oxides, whereas a strong electron localization is observed in the oxygen deficient Ga_2O_3. For further analysis, we consider the role of the crystal symmetry (Sec. III D) and the type of orbitals (s, p, or d) which form the conduction band (Sec. III E).

D. Role of the crystal symmetry

The trend in the amount of the build-up charge near the vacancy site and the resulting energy dispersion of the conduction band and associated electron group velocities (Table II) in the single-cation oxides correlate with their crystal symmetry, i.e., cubic $In_2O_3 >$ hexagonal ZnO $>$ monoclinic Ga_2O_3. A higher symmetry is expected to provide a larger orbital overlap and, hence, a better charge transport. We wish to shed some light onto this correlation.

1. Long-range symmetry: crystal anisotropy

First, let us consider the role of the long-range crystal lattice anisotropy which is exists in β-Ga_2O_3 (monoclinic phase, space group $C2/m$) due to the presence of structurally distinct (nonequivalent) Ga and O atoms. As one can see

from Table I, the effective mass anisotropy is the largest for the undoped stoichiometric β-Ga$_2$O$_3$, with the masses found to be equal to m$^{[100]}$=m$^{[010]}$=0.35 m$_e$ and m$^{[001]}$=0.32 m$_e$ within sx-LDA. However, this effective mass difference in the oxide host cannot explain the obtained strong anisotropy of the electronic properties that appears in the oxygen deficient β-Ga$_2$O$_3$ as discussed below.

Due to the presence of the nonequivalent Ga and O atoms, the distribution of the oxygen vacancies is not uniform. We find that V$_O^+$ prefers to be located in the oxygen sites of the O(1) type, while the total energy of the configuration with the defect in the O(2) or O(3) sites is higher by 163 or 267 meV, respectively. The oxygen atoms of the O(1) type form zigzag chains along the y direction with the atomic distance within the chain of 3.04 Å, while the shortest distances between the chains are 3.91 and 4.76 Å in the x and z directions, respectively. Therefore, the interaction between the oxygen vacancies distributed among the O(1) sites should be stronger within the chains than between the chains. This leads to different Fermi electron group velocities along the main crystallographic directions: we obtain 0.8×10^5, 1.9×10^5, and 1.3×10^5 m/s along the x, y, and z directions, respectively. The conductivity which is proportional to the square of the electron velocity is expected to be highly anisotropic—with the factor of 6 between the x and y directions.

Thus, we argue that crystal lattice anisotropy affects the transport properties of a TCO primarily due to a nonuniform distribution of carrier donors whereas the electronic properties of the TCO host remain nearly isotropic. For each compound, there may be a particular carrier generation mechanism found which maintains isotropic nature of the oxide host.

2. Local symmetry: oxygen coordination

As discussed in Sec. III A, the conduction band in the oxides under investigation is formed from the s orbitals of the cation and p orbitals of the oxygen atoms. These orbitals will participate in the charge transport once the materials are degenerately doped. The orbital overlap between the neighboring atoms depends on the oxygen coordination. From the symmetry considerations, an octahedral coordination provides better s-p overlap, Fig. 4, compared to a tetrahedral one. Therefore, the energy dispersion of the conduction band is expected to be larger in the case of octahedral coordination.

To elucidate the role of oxygen coordination in the charge-transport properties of the oxides, we performed calculations for the oxygen deficient high-pressure α-Ga$_2$O$_3$ phase with rhombohedral Al$_2$O$_3$-type structure (space group $R\bar{3}c$) and rock-salt ZnO phase. [In$_2$O$_3$ with $R\bar{3}c$ (corundum) and $I2_13$ structures were not considered here because the cations (anions) have the same coordination, i.e., octahedral (tetrahedral), as in bixbyite structure.]

In high-symmetry α-Ga$_2$O$_3$ phase all Ga atoms have octahedral oxygen coordination—in contrast to β-Ga$_2$O$_3$ with monoclinic $C2/m$ structure which possesses both tetragonally and octahedrally coordinated Ga atoms. We find that in the oxygen deficient α-Ga$_2$O$_3$ with V$_O^+$ concentration of 1.3
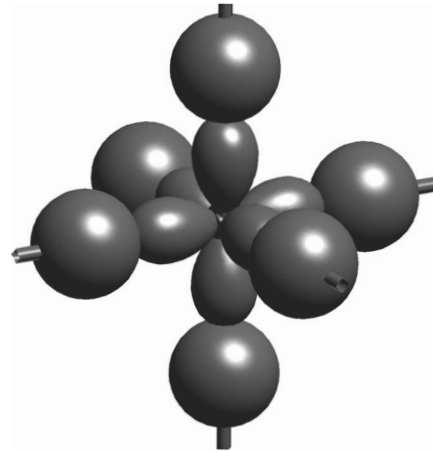

FIG. 4. Octahedral coordination of oxygen atom by cations provides the largest overlap between the s orbitals of the six metal ions and p_x, p_y, and p_z orbitals of the oxygen atom.

$\times 10^{21}$ cm^{-3}, the nearest Ga and O atoms trap 53% of the total charge density which is smaller compared to 61% in β-Ga$_2$O$_3$ with similar defect concentration of 0.8×10^{21} cm^{-3}. Consequently, the width of the single conduction band increases from 0.45 eV in β-Ga$_2$O$_3$ to 0.65 eV in α-Ga$_2$O$_3$ resulting in more than twice larger electron group velocity for the high-symmetry phase, Table II.

Similarly, we find that in oxygen deficient rocksalt ZnO with octahedral oxygen coordination of cations, the contributions from the atoms nearest to the defect decrease to 27% of the total charge density and the contributions from atoms located at different distances from the oxygen defect differ by only 2 or 3 times. Accordingly, the conduction-band width is larger (1.16 eV) that leads to a larger electron velocity near the Fermi level as compared to the ground-state hexagonal ZnO with the tetragonal oxygen coordination around Zn atoms (Table II).

Thus, we conclude that the high symmetry of octahedral oxygen coordination may improve conductivity owing to a better s-p overlap which leads to a wider conduction band and, hence, a larger electron velocity. A way to utilize the potential of an oxide is to ensure that the cations and anions possess a high *local* symmetry which can be attained via stabilization of a higher-symmetry phase or by choosing a multicomponent material with octahedral oxygen coordination for all constituents.

E. Role of cation's orbital contributions

Despite the octahedral coordination of the cations in rhombohedral Ga$_2$O$_3$, the electron velocity in the oxygen deficient material still differ by almost a factor of 3 from those in In$_2$O$_3$ and rock salt ZnO, Table II. Again, the electron effective masses of stoichiometric oxides, cf. Table I, cannot explain the differences. We extend our investigation by comparing the cation's orbital contributions to the conduction band.

As mentioned in Sec. III A, the cations and anions give nearly the same contributions at the bottom of the conduction band in all oxides investigated. Now we consider oxygen
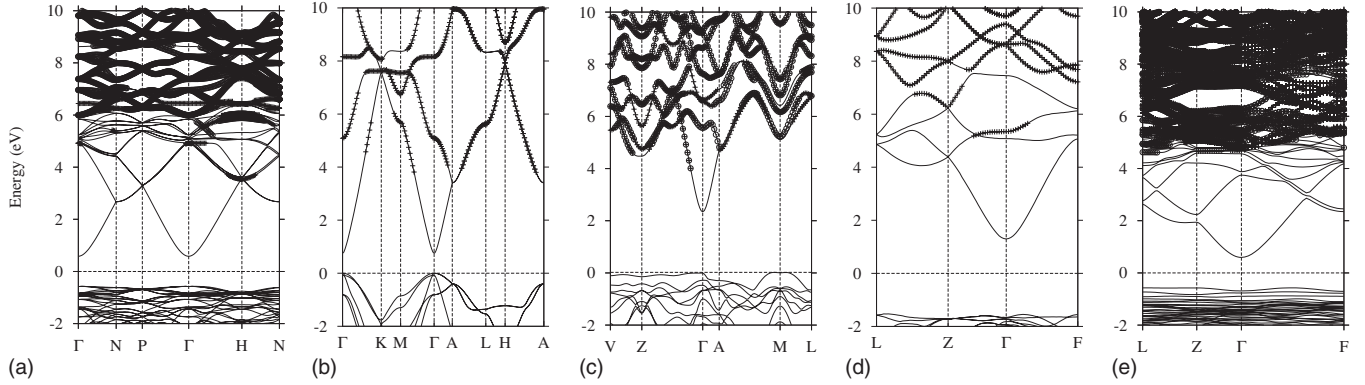
FIG. 5. Band structure of undoped stoichiometric (a) In_2O_3, (b) wurtzite ZnO, (c) β-Ga_2O_3, (d) α-Ga_2O_3, and (e) $InGaZnO_4$ as calculated within LDA. The empty p states of cation(s) are marked with (+), ($\bigcirc$), or ($\triangle$) symbols to differentiate between the structurally and/or chemically distinct cations. Remarkably, the hybrid conduction band in $InGaZnO_4$ is formed well below the detrimental Ga p states giving rise to a good charge transport.

deficient materials and analyze the orbital contributions from cations, in particular, those that are nearest to the oxygen vacancy. (The contributions from these atoms are considerable, judging by the charge build-up at the defect neighboring atoms which is observed for all oxides under investigation, see Sec. III C and Table II). Most importantly, we find that not only the s states but also the p and d states of the cations contribute to the bottom of the conduction band near the Γ point. This is expected from the $\mathbf{k} \cdot \mathbf{p}$ theory, see for example,[53] which suggests that the states located both higher (conduction states) and lower (valence states) in energy with respect to a specified band (the conduction-band minimum in our case) may contribute to that band. [Note that the sum in Eq. (1) runs over *all* bands except the conduction band.]

We compare the orbital contributions from the cations to the conduction-band wave functions in the oxygen deficient In_2O_3, rock salt ZnO, and rhombohedral Ga_2O_3. For the latter two oxides we use the high-symmetry phases where the cations have octahedral coordination. This will allow us to separate the role of local symmetry (the oxygen coordination) from the role of the electronic configuration of the cations in the observed differences in the transport properties. Values for the ground-state wurtzite ZnO and β-Ga_2O_3 are also given in Table II for clarity.

For In_2O_3 and rock salt ZnO we find that more than 80% of the nearest cation contributions comes from their s orbitals. Therefore, the conduction band originates primarily from the hybridization between the s states of the cation and the antibonding p states of the oxygen atoms. Clearly, the sp hybridization provides the most uniform charge distribution within the cell and, thus, facilitates good carrier transport.

In marked contrast to In_2O_3 and rock salt ZnO, in rhombohedral Ga_2O_3 the s orbitals of the cations located near the oxygen defect contribute only 66%, while the contributions from the Ga p states become considerable, 21% of the cations' total. This means that a substantial part of the charge introduced via the oxygen vacancy becomes trapped on the p orbitals of the neighboring Ga atoms. The charge localization occurs due to the weak hybridization (small overlap) of these highly anisotropic p orbitals with the p orbitals of the oxygen atoms from the next coordination sphere. Low crystal sym-

metry reduces this hybridization even further, as demonstrated by the results for β-Ga_2O_3 and wurtzite ZnO, Table II.

The origin of the suppressed s-orbital contributions in Ga_2O_3 and the resulting electron trapping near the defect is the proximity of the Ga p states to the conduction band bottom that gives rise to larger contributions from these p orbitals. In Fig. 5, we compare the calculated electronic band structures for undoped stoichiometric oxides where the cation's empty p states are highlighted. We find that the p states in Ga_2O_3 are located more than 1 eV closer to the bottom of the conduction band as compared to In_2O_3 and ZnO. Therefore, in contrast to indium and zinc oxides, the cation p states in Ga_2O_3 may become available for the extra electrons—as we, indeed, found.

Based on the above findings for single-cation TCOs, we can conclude that

(i) the hybridization between the cation's s orbitals and the p orbitals of the neighboring oxygen atoms is crucial for achieving good charge transport;

(ii) when the anisotropic p (or d) orbitals of the cation contribute considerably to the conduction band, the probability for the electron(s) to propagate further throughout the cell is reduced—owing to a weak hybridization between these p orbitals and the p orbitals of the neighboring oxygen atoms. As a result, the electron velocity and, hence, conductivity are reduced. The degree of reduction depends on how close in energy the cation's p (or d) states are located with respect to the bottom of the conduction band.

These findings explain the experimental observations that the conductivity of a multicomponent TCO decreases with increasing Ga content.

IV. ELECTRONIC PROPERTIES OF $InGaZnO_4$

A. Undoped stoichiometric $InGaZnO_4$

Electronic band structure investigations of undoped stoichiometric $InGaZnO_4$ have been performed earlier for the crystalline[29,30] and amorphous oxide.[63] Most importantly, it was found that despite the different band gap values of the
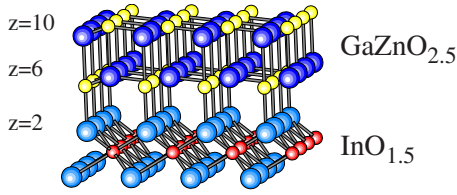
FIG. 6. (Color online) Crystal structure of InGaZnO$_4$. Only one of the three blocks which construct the conventional unit cell when stacked along the z direction, is shown. The cartesian z coordinates of the oxygen atoms are given on the left.

constituent single-cation oxides, cf. Table I, all cations give comparable contributions to the conduction band bottom of the complex oxide. Because LDA may fail in description of the empty conduction states, the above finding of the hybrid nature of the conduction band should be verified within sX-LDA. Here we performed such calculations for InGaZnO$_4$ and found that although the contributions (to the conduction band at Γ point) from In states increase—from 23% in LDA to 33% in sX-LDA, those from Ga and Zn remain the same (15%–16% and 11%, respectively) and so these states will be available for extra electrons once those are introduced into the host oxide. The change in the In contributions arises due to reduced contributions from O(1) and O(2)—namely, from 26% in LDA to 23% in sX-LDA and from 24% in LDA to 17% in sX-LDA, respectively. The reduction in the oxygen contributions is expected from a larger band gap in sX-LDA which we obtained to be equal to 3.29 eV, in good agreement with the experimental value of 3.5 eV.[10] Finally, the electron effective mass remains isotropic in sX-LDA, Table I, confirming that both structurally and chemically distinct layers, InO$_{1.5}$ and GaZnO$_{2.5}$, will participate in charge transport upon a degenerate doping of this material.

B. Spatial distribution of oxygen defect in InGaZnO$_4$

First, we investigate the spatial distribution of the oxygen vacancy in the complex layered InGaZnO$_4$ by determining the most energetically favorable location of the oxygen vacancy in the lattice. There are four structurally different sites for the defect, Fig. 6 and Table III. It can be located within the InO$_{1.5}$ layer (this corresponds to a vacancy in the O(1) structural type)[38] or GaZnO$_{2.5}$ layers [a vacancy in the O(2) site]. In addition, because Ga and Zn atoms are distributed

TABLE III. Respective total energy, in meV, of InGaZnO$_4$ system with uncompensated, partially compensated and fully compensated oxygen vacancies located at structurally different sites.

Defect location	V_O^0	V_O^+	V_O^{2+}
Within the InO$_{1.5}$ layer			
Apical Ga	+194	+138	+267
Apical Zn	0	0	0
Within the GaZnO$_{2.5}$ layers			
Apical Ga	+110	+793	+1,319
Apical Zn	+56	+536	+730

randomly in the GaZnO$_{2.5}$ layers,[40] oxygen vacancy can have either Ga^{3+} or Zn^{2+} as an apical cation, i.e., the cation in the layer adjacent to the one where the defect is located. A comparison of the total energies of the oxygen deficient systems reveals that for all three charge states of V_O, the defect prefers to be in the InO$_{1.5}$ layer having Zn as its apical atom, Table III. We note that the energy difference between the oxygen vacancy located in InO$_{1.5}$ and the one in GaZnO$_{2.5}$ layers increases significantly as the defect charge state decreases: it is only 56 meV for uncompensated V_O^0, while for partially or completely compensated defect the difference is an order of magnitude larger, Table III.

An important observation is that the energetics of different site locations of the oxygen defect in InGaZnO$_4$ correlates with the formation energy of the constituting single-cation oxides, namely, −6.42 eV/O$_2$ for In$_2$O$_3$, −7.20 eV/O$_2$ for ZnO, and −7.46 eV/O$_2$ for Ga$_2$O$_3$.[55] The most preferred location of the vacancy [i.e., the O(1) site with three In and one Zn neighbors] corresponds to the selection of the metal-oxygen bonds that would be easiest to break in order to create the defect. Although this conclusion must be verified for other systems, it may serve as initial guidance in defect studies of complex TCOs, both in crystalline and amorphous forms.

From the formation energy calculations we find that the uncompensated oxygen vacancy, V_O^0, corresponds to the ground state of the defect—similar to the In$_2$O$_3$, ZnO, and Ga$_2$O$_3$ cases, Fig. 3. The LDA-derived energy required to excite V_O^0 to obtain V_O^+ as well as the location of the oxygen defects with respect to the conduction-band bottom in InGaZnO$_4$ are also similar to the single-cation oxides, Table II. Hence, the vacancy can be photoexcited to provide a metastable conductive state. Investigations of possible charge-compensating native defects (e.g., $V_{In,Ga,Zn}$ or Zn$_{Ga}$) and defect complexes [e.g., (Zn$_{Ga}$V$_O$)] are required to further understand the lower observed conductivity in the layered InGaZnO$_4$ and in similar compounds from the series as compared to the single-cation TCOs.

Finally, the obtained preferential distribution of the oxygen vacancies in InGaZnO$_4$ may explain the observed strong anisotropy of the electrical conductivity for the layered In$_2$O$_3$(ZnO)$_n$ compounds with an increased number of ZnO layers, $n \geq 3$.[15,21,23] A larger spatial separation between the InO$_{1.5}$ layers due to extra ZnO layers may reduce the interaction between the oxygen defects which prefer to reside in the InO$_{1.5}$ layers. This will lead to a smaller electron velocity along the z direction. We note, however, that the anisotropy of the transport properties may not be well-defined in the as-grown samples since oxygen vacancy may occupy other, less favorable, locations. A higher but more anisotropic conductivity can be attained via a post-growth annealing with temperatures sufficient for the defect migration. Indeed, the observed significant decrease in the electrical conductivity along the z axis with temperature which is reported to be almost twice smaller than the conductivity within the ab plane in the high-temperature region[15] supports our conclusion.

C. Electronic properties of oxygen deficient InGaZnO$_4$

Now we analyze the conduction-band wave function in the oxygen deficient InGaZnO$_4$—similar to the studies for

single-cation oxides, see Sec. III. In accord with the hybrid nature of the bottom of the conduction band in the undoped stoichiometric $InGaZnO_4$, see Ref. 29 and Sec. IV A, all atom types in the cell give comparable contributions to the conduction band wave function: In, Ga, Zn, O(1), and O(2) atoms contribute 25%, 11%, 10%, 32%, and 22%, respectively. Moreover, for each type of atoms the contributions are fairly similar: the largest deviations are a factor of 2.5, 1.5, 2.0, 4.6, or 1.6 for, respectively, In, Ga, Zn, O(1), or O(2) located at different distances from the oxygen defect. Therefore, the charge density in the conduction band of the oxygen deficient $InGaZnO_4$ is uniformly distributed throughout the cell—similar to In_2O_3 and ZnO cases and in contrast to β-Ga_2O_3 where the defect's nearest- and next-nearest-neighbor atoms give up to two orders of magnitude smaller contributions than the rest of the cations and anions in the cell. Accordingly, for multicomponent oxide we find that the energy dispersion of the conductive band and the electron velocities near the Fermi level are comparable to those obtained for oxygen deficient In_2O_3 and superior to those for wurtzite ZnO, Table II.

For $InGaZnO_4$ we find that the charge build-up at the defect's nearest cations and next nearest anions is 37% which is notably lower than in Ga_2O_3 in either α or β phase, cf. Table II. It is important to point out that similar percentage is obtained for all locations of the oxygen defect, including the one where the vacancy has three Ga neighbors.

Further, we analyze the relative orbital contributions from the defect neighboring cations to the conduction-band wave function. We find that the s orbitals of the In and Zn atoms nearest to the vacancy located in the $InO_{1.5}$ layer or of the Ga and Zn atoms nearest to the vacancy in the $GaZnO_{2.5}$ layer contribute 82% and 74% or 75% and 71% of the cations total, respectively. The considerable increase in the s-contributions from the Ga atoms—as compared to the Ga_2O_3 phases, Table II—is attributed to the hybrid nature of the bottom of the conduction band in $InGaZnO_4$. Due to the strong hybridization between the states of *every* cation with the states of its neighboring oxygen atoms and *because of the differences in the band gaps* of the constituent oxides (3.1–3.6 eV for ZnO, 3.5–3.7 eV for In_2O_3, and 4.4–4.9 eV for Ga_2O_3, found experimentally), the hybrid band is formed well below the Ga p states, cf. Fig. 5(d). Qualitatively, this means that the interaction between the Ga s-states (conduction band) and the O p states (valence band) become weaker in $InGaZnO_4$ (band gap 3.3 eV) as compared to Ga_2O_3 (band gap ~4.6 eV), while the cation's p states remain located at about the same energy, Fig. 5. As a result, the contributions to the conduction-band wave function from these detrimental Ga p orbitals are notably smaller in $InGaZnO_4$ (14%) as compared to Ga_2O_3 (33% or 21% in β or α phase, respectively). Thus, the conduction band in complex $InGaZnO_4$ consists primarily from the cations s and the oxygen p states. This explains the obtained large electron velocity in this material, Table II.

The above results highlight an important advantage of multicomponent oxides: mixing several oxides with notably different band gaps may help overcome the charge localization effects by tuning the resulting electronic properties via chemical composition of the complex material (and, to a

lesser extent, via choosing/stabilizing a proper crystal structure). We must stress that both the relative content of the constituent oxides as well as their band gaps are critical parameters which control the resulting optical and transport properties. A large content of an oxide with a wider band gap compared to that of the other constituents may be appealing for the optical properties as well as for optimization of the material's work function desired for practical applications.[64] At the same time, however, as the band gap increases, the bottom of the hybrid conduction band will be effectively moved up—closer to the cation(s3) p states. This will increase the p orbital contribution to the conduction band and limit the carrier mobility due to the increased probability for the electrons to be trapped on the cation's p states.

V. SUBSTITUTIONAL DOPING IN $InGaZnO_4$

Targeted doping with specific impurities which donate extra electrons upon aliovalent substitution represents an alternative route for the carrier generation in TCO hosts. Compared to the native point defects such as oxygen vacancy, substitutional doping is more appealing due to better stability of the doped samples to the environment that is essential for practical applications. Among single-cation oxides, the most studied and commercially utilized are Sn-doped In_2O_3, Al-doped ZnO, Sb-doped SnO_2, F-doped ZnO and SnO_2. To the best of our knowledge, there were no reports on substitutional doping of $InGaZnO_4$ or other materials from the homologous series left [in Ref. 15, $(ZnO)_mIn_2O_3$ was doped with Ca^{2+}, Sr^{2+}, and Ba^{2+} to improve the thermoelectric properties].

One of the main challenges of substitutional doping in a multicomponent oxide is to find a proper dopant which will donate extra electron(s) and lead to degenerate doping. The valence and the ionic size of both the dopant and all the cations in the cell should be taken into consideration. For example, doping of $InGaZnO_4$ with Al, which is known to be a good choice in the case of ZnO, is likely to result in Al^{3+} (the ionic radius is 0.53 Å) substituting Ga^{3+}(0.61 Å) instead of Zn^{2+}(0.74 Å) so that the extra electrons are not generated and the material remains nonconducting. Moreover, nonuniform spatial distribution of the dopants, their clustering or secondary phase formation as well as formation of defect complexes may become more pronounced in multicomponent oxides due to complexity and peculiarities in their crystal structure as compared to their single-cation counterparts. Systematic theoretical investigations may prove to be valuable to guide future experiments.

Our goal is to investigate the structural, electronic and optical properties of doped $InGaZnO_4$ and also to compare them with those obtained for the oxygen deficient material. We begin by studying Sn^{4+} and Ga^{3+} substitutions. The former dopant is the most intuitive choice, while extra Ga may be considered as an intrinsic stoichiometry defect. In addition to these "traditional" dopants, we also considered Ti^{4+} and Zr^{4+} ions—following recent experimental and theoretical findings that transition metal dopants provide an enhanced carrier mobility which leads to a pronounced increase in conductivity with no changes in spectral transmittance.[61,65,66]

TABLE IV. Properties of substitutionally doped InGaZnO$_4$. The dopant ionic radius, R, in Å; the optimized distances between the dopant and its oxygen neighbors, D(M-O), in Å; the formation energy of the defect, E_{form}, in eV; the electron velocities, v, calculated along the main crystallographic directions in the vicinity of the Fermi level; the density of states at the Fermi level, N(E_F), in states/eV·cell; the fundamental band gap, $E_{fundamental}$, in eV; the BM shift (the Fermi energy displacement measured from the bottom of the conduction band), in eV, for Ga, Sn, Ti, and Zr doped InGaZnO$_4$. The dopant concentration is 1.75×10^{21} cm^{-3} in all materials. For comparison, the ionic radii of In and Zn are 0.94 and 0.74 Å, respectively.

	Ga$_{Zn}$	Sn$_{In}$	Ti$_{In}$	Zr$_{In}$
R	0.61	0.83	0.75	0.86
D(M-O)	1.88–2.16	2.09–2.15	1.98–2.10	2.05–2.45
E_{form}	−0.32	0.62	−2.79	−3.92
$v^{[100]} \times 10^5$ m/s	8.56	8.18	4.93	7.89
$v^{[010]} \times 10^5$ m/s	8.69	8.11	5.32	8.17
$v^{[001]} \times 10^5$ m/s	8.75	8.52	5.79	8.12
N(E_F)	2.2	2.4	6.3	2.3
N(E_F)v^2	3.63	3.65	3.97	3.31
$E_{fundamental}$	1.26	1.20	1.43	1.48
BM shift	1.51	1.45	1.07	1.41

A. Site location of Sn, Ga, Ti, or Zr in InGaZnO$_4$

First, we determine which cation in the host structure is most likely to be substituted by the particular dopant. For this, we compare the energies of the relaxed structures where In or Zn is substituted by Sn or Ga; and In, Ga, or Zn is substituted by Ti or Zr. Other configurations, e.g., Sn substituted on Ga sites, were not considered due to the large ionic radius mismatch. From the calculations of the defect formation energies, we find that Sn, Ti, and Zr have a strong preference to substitute In atoms whereas the substitution of Ga or Zn atoms corresponds to a higher energy by at least 1.4, 1.3, and 3.6 eV, respectively. [The formation energies are $E_{form}(Sn_{Zn})$=2.03 eV, $E_{form}(Ti_{Ga})$=−1.44 eV, $E_{form}(Ti_{Zn})$= −1.52 eV, $E_{form}(Zr_{Ga})$=−0.29 eV, and $E_{form}(Zr_{Zn})$= −0.33 eV. These should be compared to the formation energies given in Table IV]. The obtained preferential substitution can be understood based on the local symmetry arguments: ions with larger positive charge (M^{4+} in our case) prefer to have more oxygen neighbors and so the octahedral oxygen coordination (In sites) is more favorable than the tetrahedral one (Zn or Ga sites). Here we note that the obtained formation energies for doped InGaZnO$_4$ are similar to those in doped In$_2$O$_3$. For the latter, we find the formation energy of the Sn substitution into In site to be equal to 0.17 eV (which is in agreement with Ref. 58), whereas for the Ti substitution E_{form}=−2.92 eV.

In contrast, Ga shows a preference to substitute Zn atoms with the energy for In substitution being only 0.05 eV higher [$E_{form}(Ga_{In})$=−0.27 eV which should be compared to the value for Ga$_{Zn}$, cf. Table IV]. Because of the relatively small energy difference, one can expect that some of the extra Ga ions may substitute In atoms upon growth at elevated tem-

peratures. This is a disadvantage since Ga has the same valence as In and so it will not contribute extra electrons upon the substitution.

In Table IV, the optimized distances between the dopant and its nearest oxygen neighbors are compared for doped InGaZnO$_4$—along with the calculated electron velocities and the optical properties to be discussed in Sec. V C.

B. Electronic properties of doped InGaZnO$_4$

We find that the electron velocity, Table IV, is nearly isotropic in all doped materials—despite the nonuniform distribution of the dopants which prefer to reside within the InO$_{1.5}$ layers. This is in accord with the hybrid nature of the conduction band in InGaZnO$_4$ discussed above (see Sec. IV) and in our earlier work.^{29} Indeed, in the Sn, Zr, and Ga doped cases, the net contributions to the conduction band wave function from the atoms that belong to either In-O or Ga-Zn-O layers are similar, namely, 58% or 42% in Sn case, 51% or 49% in Ga and Zr cases, respectively. Furthermore, compared to the oxygen deficient material, see Sec. IV C, the charge density in the conduction band of the Sn, Zr, and Ga doped InGaZnO$_4$ is more uniformly distributed throughout the cell since the largest deviations in the atomic contributions are only a factor of 1.2–1.6, 1.4–1.5, 1.1–1.4, 1.2–1.7, and 1.1–1.6 for, respectively, In, Ga, Zn, O(1), and O(2) located at different distances from the dopant. [Note that similar to the oxygen reduced complex oxides of the InGaO$_3$(ZnO)$_n$ family, the isotropic behavior may not be maintained in substitutionally doped materials with the increased number of ZnO layers (n) and anisotropic transport properties may appear after annealing.]

The more uniform charge density distribution in the conduction band of Sn, Ga, and Zr doped InGaZnO$_4$ leads to almost twice larger electron velocities ($\sim 8 \times 10^5$ m/s) than in the oxygen deficient material (4×10^5 m/s) with the concentration of the partially compensated oxygen defect of 1.75×10^{21} cm^{-3}. (In this case, we compare the same defect concentration, with Sn or V$_O^+$ giving one extra electron per impurity or per defect.) Similar results are obtained for Sn-doped In$_2$O$_3$ where the electron velocity is 1.4 times larger (9.17×10^5 m/s for the dopant concentration of 1.93×10^{21} cm^{-3}) as compared to the oxygen deficient indium oxide (6.42×10^5 m/s for 1.96×10^{21} cm^{-3}). One should take into account the *carrier* concentration in each case which is determined by the corresponding density of states (DOS) in the vicinity of the Fermi level. The DOS(E_F) increases when the energy dispersion of the conduction band decreases which represents a more localized state. The conductivity σ depends on both, the electron group velocity and the density of states near Fermi

$$\sigma = \frac{2e^2}{\Omega} \sum_{k\lambda} |v_{k\lambda}|^2 \tau_{k\lambda} \delta(E_{k\lambda} - E_F). \qquad (3)$$

Here e is the electron charge, Ω—the volume of the Brillouin zone, k—the wave vector, λ—the band index, v—the electron group velocity, and E_F is the Fermi energy. Based on our calculations, we can estimate the band-structure conductivity factor—the square of the electron velocity by the density of

states, Eq. (3). The estimates suggest that the difference between oxygen deficient and Sn-doped oxides, $InGaZnO_4$ and In_2O_3, are almost negligible. Therefore, the relaxation time for the Fermi surface electrons, τ, will play crucial role in determining the resulting conductivity. While we cannot estimate τ directly from the band-structure calculations, below we speculate about the scattering mechanism associated with the Coulomb interaction between the ionized donor impurities and free electrons. (We do not consider the effects of grain boundaries, structural disorder and neutral impurities—which may have a significant effect on the transport properties.)

According to Refs. 67–69 the relaxation time depends on the concentration of impurity centers, N_i, which have charge Ze as well as the free electron density n. Because the charge state of the Sn^{4+} substituting In^{3+} ions, i.e., of the Sn defect, is the same as for the partially compensated oxygen vacancy, V_O^+, there is no apparent difference in the relaxation times for the two carrier generation mechanisms ($Z=1$ and $N_i=n$ for both). However, we find that the structural relaxation is significantly stronger around the oxygen defect than near the substitutional dopant. For In_2O_3, the displacement of the nearest neighbor atoms from their original positions is 0.084 Å and uniform around Sn ions, while it is much stronger and anisotropic around the partially compensated oxygen vacancy with the displacements of 0.081, 0.112, 0.127, and 0.160 Å for the four nearest neighbor In atoms. For $InGaZnO_4$, the nearest neighbor displacements are 0.069–0.084 Å in Sn-doped material and 0.097–0.331 Å in the oxygen deficient oxide. Qualitatively, the larger atomic displacements around the defect are expected to give rise to significantly stronger scattering in the oxygen reduced oxides as compared to the substitutionally doped materials. Most importantly, a strong Coulomb attraction between the V_O^+ defects and the free carriers and, hence, a short electron relaxation time, should be expected in all oxides considered in this work, since the partially compensated oxygen vacancy corresponds to a metastable state.

Thus, proper doping with aliovalent substitutional impurities is expected to lead to a notably higher electron mobility and conductivity than those observed in the oxygen reduced oxides.

C. Role of the dopant's electronic configuration

To elucidate the differences in the calculated electron velocities in Ga, Sn, Ti and Zr-doped $InGaZnO_4$, cf. Table IV, we compared the relative atomic contributions to the conduction band wave functions in these materials. First we find that in the Ga, Sn, and Zr cases, the anions give larger net contributions (64%–66%) compared to the cations (34%–36%), while in the case of the Ti doping the cations contribute twice as much (62%) to the total charge in the cell. Moreover, in Ti-doped $InGaZnO_4$ about 64% of the net *cations'* contribution is due to the Ti d states. In contrast, the states of Sn, Ga (primarily s states) or Zr (primarily d states) give only 18%, 5%, or 7% of the total contributions from all cations in the cell. Therefore, the extra charge associated with the aliovalent substitution is uniformly distributed throughout the cell in Sn, Ga, and Zr-doped $InGaZnO_4$, while it is mostly localized on the d states of Ti (Ref. 70) resulting in the significantly lower electron velocity in the Ti-doped $InGaZnO_4$. However, taking into account the increased density of states in the latter case, the band-structure conductivity factor, $N(\epsilon)v^2(\epsilon)$, cf. Eq. (3), is approximately similar for all dopants investigated, with Ti showing the largest contribution to the band-structure conductivity, Table IV.

Further, we investigate how the dopant's electronic configuration and ionic radius affect the optical properties of $InGaZnO_4$. In Table IV, the fundamental band gap and the Burstein-Moss (BM) shift[71] are compared for doped materials. The fundamental band gap is measured between the top of the valence band and the bottom of the conduction band (i.e., at Γ point), while the optical band gap in doped materials corresponds to the energy transitions from the top of the valence band to the Fermi level and, hence, is equal to the fundamental band gap plus the Fermi energy displacement (the BM shift). Note that, in contrast to oxygen deficient $InGaZnO_4$, the substitutionally doped material does not exhibit a second gap, as expected from hybridization between the dopant's states with the p states of neighboring oxygen atoms.

We find that the BM shift is ∼0.4 eV smaller for the Ti-doped $InGaZnO_4$ as compared to Ga, Sn, or Zr, Table IV, although Ti^{4+} provides the same number of extra electrons per substitution of In^{3+} as Sn^{4+} or Zr^{4+} (or as the substitution of Zn^{2+} with Ga^{3+}). This is explained by the significant charge localization on the Ti d states located in the vicinity of the Fermi level.[70] The smaller BM shift should not affect the optical transparency within the visible range: because the band gap in $InGaZnO_4$ is large enough, 3.5 eV,[10] the energy of the transitions from the valence band is above the visible range (i.e., above 3.1 eV) even in the undoped oxide.

Moreover, we argue that a smaller BM shift associated with the electron localization on the dopant d states allows one to balance the optical and transport properties more efficiently.[61] In a conventional TCO, e.g., Sn-doped In_2O_3, an increased carrier concentration desired for an improved conductivity comes at a cost of an increased optical absorption because a pronounced BM shift reduces the energy of the transitions from the Fermi level, i.e., from the partially occupied conduction band. In addition, plasma oscillations may affect the optical properties by reflecting the electromagnetic waves of frequency below that of the plasmon. In contrast to the conventional (non-d element) doping, transition metal dopants may allow one to introduce large carrier concentrations without compromising on the optical transparency. Indeed, smaller BM shift in Ti-doped $InGaZnO_4$ implies that the impurity concentration can be increased further (up to as high as $1.22 \cdot 10^{22}$ cm^{-3}, based on our electronic band structure estimates) before reaching the same energy of the optical transitions from the Fermi level as with Ga, Sn, or Zr doping at the dopant concentration of $1.75 \cdot 10^{21}$ cm^{-3}. We stress here that the above estimates are only to emphasize the trend between the s and d dopants. In a viable TCO, the impurity concentration is limited by ionized impurity scattering on the electron donors as well as by the plasma frequency.

Very recently, the experimental results for Mn doped $InGaZnO_4$ were reported.[72] It was found that the conductiv-

ity decreases while the carrier mobility increases with Mn content (up to 2.5 at.% of Mn). Such an intriguing behavior may be associated with the onset of the long-range magnetic interactions between the Mn ions that leads to significantly longer relaxation time for the carriers of a particular spin.[61] At the same time, the density of states near the Fermi level, and thus, the *carrier* concentration, decreases once the stable magnetic configuration is achieved. Accurate band structure calculations which go beyond LDA to correct the band gap value and the position of the localized Mn d states with respect to band edges should be performed to verify this supposition.

D. Charge compensation with interstitial oxygen

It is known that high oxygen pressure can significantly reduce the conductivity of doped oxides due to the formation of neutral complexes between the ionized dopants and the interstitial oxygen atoms.[56,73,74] Indeed, it was shown[61] that interstitial oxygen in Mo-doped In_2O_3 may significantly affect the electronic, magnetic, and optical properties of the material. However, the formation energy of the O_i defect in undoped In_2O_3 is very high (we obtained $E_{form}=8.88$ eV for the oxygen-rich conditions that is in agreement with Ref. [58]). For a dopant—interstitial-oxygen defect complex (e.g., $Mo_{In}^{\bullet\bullet\bullet}O_i''$)$^\bullet$—given in Kroger-Vink notations, the energy of formation is lower by about 3 eV as compared to the interstitial oxygen alone.[61]

Given its compositional and structural complexity, $InGaZnO_4$ is a good test structure for investigation of the charge compensation mechanism via oxygen interstitial. Significantly, we find that the formation energy of the neutral O_i'' defect in the multicomponent oxide is 4.77 eV which is almost twice lower than that in In_2O_3. This suggests that the formation of dopant-O_i defect complexes in $InGaZnO_4$ is possible. While studies of particular dopants and defect complexes in $InGaZnO_4$ are beyond the scope of this work, here we would like to understand the preferred distribution of the interstitial oxygen atoms in the complex oxide with chemically and structurally distinct layers. For this, we performed calculations for the undoped $InGaZnO_4$ with extra oxygen atom located in various structurally nonequivalent sites in the lattice. We find nine such positions for O_i which we divide into three groups according to their optimized Cartesian z coordinate: (i) the first three of them (cases 1, 2, and 3 in Table V) have $z=3.0-3.1$ which is slightly above the framework oxygen atoms in the $InO_{1.5}$ layer with $z=1.9-2.2$, cf. Fig. 6; (ii) another three with $z=9.3$ (cases 4 and 5) and $z=7.3$ (case 6) are within the $GaZnO_{2.5}$ double layer where the framework oxygen atoms have $z=6.2-6.5$ and $z=9.9-10.2$; (iii) the remaining three with $z=4.7-5.5$ (cases 7, 8, and 9) reside in the "shared" space between the structurally and chemically different layers, and are about 2.5 times closer to the $GaZnO_{2.5}$ layer.

Table V lists the respective total energies and the optimized distances between the interstitial oxygen and its nearest cations for the structures with different location of the defect. As one can see, the interstitial oxygen prefers to reside within the $InO_{1.5}$ layer having the distance of ~2.1 Å

TABLE V. Optimized distances between the interstitial oxygen and its nearest cation neighbors, in Å, and the respective total energy ΔE, in meV, for $InGaZnO_4$ systems with O_i located in various positions. The division into the groups is made based on the optimized cartesian z coordinate, see text and Fig. 6.

	Nearest-neighbor cations			ΔE
$InO_{1.5}$ layer				
1 $z=3.1$	Ga1.87	In2.14	In2.99	0
2 $z=3.1$	Ga1.88	In2.15	In2.92	+22
3 $z=3.0$	Zn1.92	In2.11	In2.91	+11
$GaZnO_{2.5}$ layers				
4 $z=9.4$	Ga1.85	Ga2.04	Zn2.46	+112
5 $z=9.3$	Zn1.91	Zn2.03	Ga2.31	+253
6 $z=7.3$	Zn1.90	Zn1.96	Ga2.49	+72
In between/shared				
7 $z=5.1$	Ga1.87	Zn1.89	Zn1.90	+1,490
8 $z=4.7$	Ga1.84	In2.33	Zn2.43	+127
9 $z=5.5$	Ga1.89	Ga1.89	In2.91	+447

from one of the In atoms (cases 1, 2, and 3). The total energy deviates insignificantly when the next-nearest neighbor is either Ga or Zn. When the distance between the O_i and In atom increases (to 2.3, 2.9, and 3.2 Å) so does the total energy (by 127, 447, and 1,490 meV, respectively). The energy decreases, however, when the interstitial oxygen atoms reside within the $GaZnO_{2.5}$ layers. Nonetheless, the energy difference between the structures with O_i located within the $InO_{1.5}$ or $GaZnO_{2.5}$ layers is at least 50 meV. Because the substitutional dopants also have a preference to reside within the $InO_{1.5}$ layers, as shown above, the formation of the charge compensated complexes is likely. Therefore, the ambient oxygen pressure must be carefully controlled to avoid the charge compensation and to ensure that the largest carrier concentration per substitutional dopant is attained. Using dopants which donate more than one electron per substitution, such as Mo^{6+}, (Ref. [61]) represents an alternative route to mitigate the charge compensation and, thus, to achieve good electrical conductivity.

VI. CONCLUSIONS

The results of our comparative electronic band structure investigations of In_2O_3, ZnO, Ga_2O_3, and $InGaZnO_4$ allow us to draw several important conclusions:

(1) The electronic and optical properties of the oxides originate from the strong interaction between the metal s orbitals and the p orbitals of the neighboring oxygen atoms. Due to the Ms-Op overlap, the undoped stoichiometric oxides exhibit large band gaps (3.4–4.9 eV) and small electron effective masses (0.28–0.35 m_e). The latter, however, cannot explain the differences in the observed electrical conductivities in degenerately doped oxides.

(2) Due to the three-dimensional Ms-Op network, all undoped stoichiometric oxides, including those with well-defined *crystal lattice anisotropy*, are capable to give rise to

(nearly) isotropic conductivity. In layered $InGaZnO_4$, the electron effective masses are the same within and across the structurally and chemically distinct layers, as confirmed by our sX-LDA calculations.

However, long-range structural anisotropy favors nonuniform (preferential) distribution of carrier donors. In β-Ga_2O_3, oxygen vacancies are most likely to appear at the O(1) sites which form zigzag chains along the y axis leading to a twice larger electron velocity in this direction. In $InGaZnO_4$, an oxygen vacancy, interstitial oxygen atom and substitutional Sn, Zr, and Ti prefer to reside within the $InO_{1.5}$ layer that may explain the observed temperature-dependent anisotropy of the electrical conductivity in $InGaO_3(ZnO)_n$ and $In_2O_3(ZnO)_n$ with an increased number of ZnO layers, n.

(3) *Octahedral oxygen coordination* provides the largest sp overlap, giving rise to a 1.6 and 2.5 times larger electron velocity in hypothetical oxygen deficient rock salt ZnO and α-Ga_2O_3 as compared to wurtzite ZnO and β-Ga_2O_3, respectively. Therefore, a way to improve conductivity and to utilize the potential of an oxide is to ensure that the cations and anions possess a high *local* symmetry which can be attained via stabilization of a higher-symmetry phase or by choosing a multicomponent material with, preferably, octahedral oxygen coordination for all constituents.

(4) Most significantly, we find that the electronic configuration of cation(s), in particular, the energy proximity of its *empty p-states* with respect to the CBM, plays the key role in determining the transport properties of oxygen deficient materials. In β-Ga_2O_3, the Ga p states are energetically compatible with the s states of the host cations and, thus, available for the vacancy-induced electrons. As a result, in marked contrast to In_2O_3 and ZnO, the carriers become trapped on the p states of the Ga atoms nearest to the defect—owing to the weak hybridization of these highly anisotropic Ga p orbitals with the p orbitals of their neighboring oxygen atoms.

This finding explains why β-Ga_2O_3 is not a viable TCO and also suggests that a large content of Ga_2O_3 in a multicomponent TCO may lead to a suppressed conductivity—unless an alternative carrier generation mechanism is found.

(5) Due to the hybrid nature of the conduction band, multicomponent oxides offer a possibility to overcome the detrimental electron localization effects by tuning the resulting electronic—as well as optical—properties via chemical composition.

(6) In all oxides investigated in this work, neutral oxygen vacancy, V_O^0, results in a fully occupied, thus, nonconducting state located well below the oxide conduction band minimum. Because V_O^0 also corresponds to the ground state of the defect, a conducting behavior may appear only if the vacancy is excited to V_O^+. In In_2O_3, ZnO and $InGaZnO_4$, our LDA estimates suggest that the energy of excitation is within the visible range, i.e., the vacancy can be photoexcited, leading to a metastable conductive state. In β-Ga_2O_3, the excitation is highly unlikely because V_O^0 and V_O^+ prefer to be located at the different oxygen sites—of type O(3) and O(1), respectively.

(7) Aliovalent substitutional doping with next-column elements gives rise to twice larger electron velocity as compared to oxygen deficient materials. However, the carrier concentration is expected to be lower in the former due to a smaller [by order(s) of magnitude] density of states in the vicinity of the Fermi level. This is associated with a nearly rigid-band shift of the Fermi level upon substitutional doping, whereas notable electron localization near the oxygen vacancy leads to a higher DOS near the Fermi level in oxygen deficient materials.

Our results suggest that the differences in the conductivities in oxygen deficient and doped oxides stem from different carrier relaxation time. A shorter τ in oxygen deficient oxides is expected from a significant atomic relaxation around the oxygen defect and a stronger Coulomb attraction between the oxygen vacancy V_O^+ and the free carriers.

(8) Doping with specific transition metal elements represents an efficient way to achieve high electrical conductivity without substantial changes in the spectral transmittance. In addition, it provides a possibility to tune the electronic and optical properties of oxide via the formation of charged defect complexes with interstitial oxygen atom.

Thus, in-depth understanding of the microscopic properties of the post-transition metal oxides provides significant insights into the underlying phenomena in the conventional TCOs. Moreover, our systematic studies reveal several ways to knowledgeably manipulate the resulting properties—by tuning the chemical composition of complex hosts and carefully choosing proper carrier generation mechanisms—to give rise to broader application range of these unique materials.

*juliaem@mst.edu

[1] R. D. Shannon, J. L. Gillson, and R. J. Bouchard, J. Phys. Chem. Solids **38**, 877 (1977).

[2] K. L. Chopra, S. Major, and D. K. Pandya, Thin Solid Films **102**, 1 (1983).

[3] A. L. Dawar and J. C. Joshi, J. Mater. Sci. **19**, 1 (1984).

[4] MRS Bull. 25 (2000), special issue on transparent conducting oxides, edited by D. S. Ginley and C. Bright.

[5] H. Kawazoe and K. Ueda, J. Am. Ceram. Soc. **82**, 3330 (1999).

[6] B. J. Ingram, G. B. Gonzalez, D. R. Kammler, M. I. Bertoni, and T. O. Mason, J. Electroceram. **13**, 167 (2004).

[7] H. Un'no, N. Hikuma, T. Omata, N. Ueda, T. Hashimoto, and H.

Kawazoe, Jpn. J. Appl. Phys. **32**, L1260 (1993).

[8] J. M. Phillips, J. Kwo, and G. A. Thomas, Appl. Phys. Lett. **65**, 115 (1994).

[9] A. J. Freeman, K. R. Poeppelmeier, T. O. Mason, R. P. H. Chang, and T. J. Marks, MRS Bull. **25**, 45 (2000).

[10] M. Orita, M. Takeuchi, H. Sakai, and H. Tanji, Jpn. J. Appl. Phys. **34**, L1550 (1995).

[11] K. Nomura, H. Ohta, K. Ueda, T. Kamiya, M. Hirano, and H. Hosono, Science **300**, 1269 (2003).

[12] K. Nomura, H. Ohta, A. Takagi, T. Kamiya, M. Hirano, and H. Hosono, Nature (London) **432**, 488 (2004).

[13] H. Hiramatsu, H. Ohta, W. S. Seo, and K. J. Koumoto, J. Jpn. Soc. Powder Powder Metall. **44**, 44 (1997).

[14] M. Kazeoka, H. Hiramatsu, W. S. Seo, and K. Koumoto, J. Mater. Res. **13**, 523 (1998).

[15] H. Kaga, R. Asahi, and T. Tani, Jpn. J. Appl. Phys. **43**, 3540 (2004); **43**, 7133 (2004).

[16] K. Nomura, T. Kamiya, H. Ohta, T. Uruga, M. Hirano, and H. Hosono, Phys. Rev. B **75**, 035212 (2007).

[17] J. L. F. Da Silva, Y. Yan, and S.-H. Wei, Phys. Rev. Lett. **100**, 255501 (2008).

[18] W.-J. Lee, E.-A. Choi, J. Bang, B. Ryu, and K. J. Chang, Appl. Phys. Lett. **93**, 111901 (2008).

[19] D.-Y. Cho, J. Song, K. D. Na, C. S. Hwang, J. H. Jeong, J. K. Jeong, and Y.-G. Mo, Appl. Phys. Lett. **94**, 112112 (2009).

[20] W. Lim, E. A. Douglas, S.-H. Kim, D. P. Norton, S. J. Pearton, F. Ren, H. Shen, and W. H. Chang, Appl. Phys. Lett. **94**, 072103 (2009).

[21] A. Walsh, J. L. F. Da Silva, Y. Yan, M. M. Al-Jassim, and S.-H. Wei, Phys. Rev. B **79**, 073105 (2009).

[22] A. Walsh, J. L. F. Da Silva, and S.-H. Wei, Chem. Mater. **21**, 5119 (2009).

[23] H. Hiramatsu, W. S. Seo, and K. J. Koumoto, Chem. Mater. **10**, 3033 (1998).

[24] T. Moriga, D. R. Kammler, T. O. Mason, G. B. Palmer, and K. R. Poeppelmeier, J. Am. Ceram. Soc. **82**, 2705 (1999).

[25] M. Orita, H. Ohta, M. Hirano, S. Narushima, and H. Hosono, Philos. Mag. B **81**, 501 (2001).

[26] H. Kawazoe, N. Ueda, H. Un'no, T. Omata, H. Hosono, and H. Tanoue, J. Appl. Phys. **76**, 7935 (1994).

[27] H. Mizoguchi and P. M. Woodward, Chem. Mater. **16**, 5233 (2004).

[28] M. Orita, H. Tanji, M. Mizuno, H. Adachi, and I. Tanaka, Phys. Rev. B **61**, 1811 (2000).

[29] J. E. Medvedeva, Europhys. Lett. **78**, 57004 (2007).

[30] H. Omura, H. Kumomi, K. Nomura, T. Kamiya, M. Hirano, and H. Hosono, J. Appl. Phys. **105**, 093712 (2009).

[31] E. Wimmer, H. Krakauer, M. Weinert, and A. J. Freeman, Phys. Rev. B **24**, 864 (1981).

[32] M. Weinert, E. Wimmer, and A. J. Freeman, Phys. Rev. B **26**, 4571 (1982).

[33] D. M. Bylander and L. Kleinman, Phys. Rev. B **41**, 7868 (1990).

[34] A. Seidl, A. Görling, P. Vogl, J. A. Majewski, and M. Levy, Phys. Rev. B **53**, 3764 (1996).

[35] R. Asahi, W. Mannstadt, and A. J. Freeman, Phys. Rev. B **59**, 7486 (1999).

[36] C. B. Geller, W. Wolf, S. Picozzi, A. Continenza, R. Asahi, W. Mannstadt, A. J. Freeman, and E. Wimmer, Appl. Phys. Lett. **79**, 368 (2001).

[37] M. Y. Kim, R. Asahi, and A. J. Freeman, J. Comput. Aided Mater. Des. **9**, 173 (2002).

[38] K. Kato, I. Kawada, N. Kimizuka, and T. Katsura, Z. Kristallogr.. **141**, 314 (1975).

[39] N. Kimizuka and T. Mohri, J. Solid State Chem. **60**, 382 (1985).

[40] C. Li, Y. Bando, M. Nakamura, and M. Kimizuka, J. Electron Microsc. (Tokyo) **46**, 119 (1997).

[41] J. E. Medvedeva, in *Transparent Electronics: From Synthesis to Applications*, edited by A. Facchetti and T. Marks (Wiley, New York, 2010).

[42] J. E. Medvedeva and A. J. Freeman, Europhys. Lett. **69**, 583 (2005).

[43] S. Jin, Y. Yang, J. E. Medvedeva, J. R. Ireland, A. W. Metz, J. Ni, C. R. Kannewurf, A. J. Freeman, and T. J. Marks, J. Am. Chem. Soc. **126**, 13787 (2004).

[44] Y. Yang, S. Jin, J. E. Medvedeva, J. R. Ireland, A. W. Metz, J. Ni, M. C. Hersam, A. J. Freeman, and T. J. Marks, J. Am. Chem. Soc. **127**, 8796 (2005).

[45] S. Jin, Y. Yang, J. E. Medvedeva, L. Wang, S. Li, N. Cortes, J. R. Ireland, A. W. Metz, J. Ni, M. C. Hersam, A. J. Freeman, and T. J. Marks, Chem. Mater. **20**, 220 (2008).

[46] R. L. Weiher and R. P. Ley, J. Appl. Phys. **37**, 299 (1966).

[47] I. Hamberg, C. G. Granqvist, K. F. Berggren, B. E. Sernelius, and L. Engström, Phys. Rev. B **30**, 3240 (1984).

[48] A. Walsh, J. L. F. Da Silva, S.-H. Wei, C. Körber, A. Klein, L. F. J. Piper, A. De Masi, K. E. Smith, G. Panaccione, P. Torelli, D. J. Payne, A. Bourlange, and R. G. Egdell, Phys. Rev. Lett. **100**, 167402 (2008).

[49] F. Fuchs and F. Bechstedt, Phys. Rev. B **77**, 155107 (2008).

[50] C. Klingshirn, Phys. Status Solidi B **71**, 547 (1975).

[51] H. H. Tippins, Phys. Rev. **140**, A316 (1965).

[52] N. Ueda, H. Hosono, R. Waseda, and H. Kawazoe, Appl. Phys. Lett. **71**, 933 (1997).

[53] N. W. Ashcroft and N. D. Mermin, *Solid State Physics* (W.B. Saunders, Philadelphia, 1976).

[54] J. E. Medvedeva, E. N. Teasley, and M. D. Hoffman, Phys. Rev. B **76**, 155107 (2007).

[55] T. B. Reed, *Free energy of Formation of Binary Compounds* (MIT Press, Cambridge, Massachusetts, 1971).

[56] J. H. W. De Wit, G. van Unen, and M. Lahey, J. Phys. Chem. Solids **38**, 819 (1977).

[57] F. A. Kröger, *The Chemistry of Imperfect Crystals* (North-Holland, Amsterdam, 1974).

[58] S. Lany and A. Zunger, Phys. Rev. Lett. **98**, 045501 (2007).

[59] Consistently, a fully compensated oxygen vacancy results in a non-conductive state with the Fermi level located within the fundamental band gap, i.e., between the valence and the conduction bands.

[60] The results of the screened-exchange LDA will be published elewhere.

[61] J. E. Medvedeva, Phys. Rev. Lett. **97**, 086401 (2006).

[62] O. N. Mryasov and A. J. Freeman, Phys. Rev. B **64**, 233111 (2001).

[63] T. Kamiya, K. Nomura, and H. Hosono, Phys. Status Solidi A **206**, 860 (2009).

[64] K. Inoue, K. Tominaga, T. Tsuduki, M. Mikawa, and T. Moriga, Vacuum **83**, 552 (2008).

[65] Y. Meng, X. Yang, H. Chen, J. Shen, Y. Jiang, Z. Zhang, and Z. Hua, Thin Solid Films **394**, 219 (2001); J. Vac. Sci. Technol. A **20**, 288 (2002).

[66] Y. Yoshida, D. M. Wood, T. A. Gessert, and T. J. Coutts, Appl.

Phys. Lett. **84**, 2097 (2004).

[67] R. B. Dingle, Philos. Mag. **46**, 831 (1955).

[68] H. Brooks, Adv. Electron. Electron Phys. **7**, 85 (1955).

[69] J. R. Bellingham, W. A. Phillips, and C. J. Adkins, J. Mater. Sci. Lett. **11**, 263 (1992).

[70] Note that in contrast to Ti-doped $InGaZnO_4$ where the Ti d states are located 0.15 eV above the Fermi level, the Zr d states are significantly higher in energy, namely, $\sim$1.0 eV above the Fermi level, and thus are not available for the extra electrons.

[71] E. Burstein, Phys. Rev. **93**, 632 (1954); T. S. Moss, Proc. Phys. Soc. B **67**, 775 (1954).

[72] S.-J. Liu, H.-W. Fang, S.-H. Su, C.-H. Li, J.-S. Cherng, J.-H. Hsieh, and J.-Y. Juang, Appl. Phys. Lett. **94**, 092504 (2009).

[73] G. Frank and H. Köstlin, Appl. Phys. A: Mater. Sci. Process. **27**, 197 (1982).

[74] G. B. González, J. B. Cohen, J. Hwang, T. O. Mason, J. P. Hodges, and J. D. Jorgensen, J. Appl. Phys. **89**, 2550 (2001).